JOURNAL OF AIRCRAFT
Vol. 44, No. 6, November–December 2007

Parametric Studies on Ground Vibration Test Modeling for Highly Flexible Aircraft

Chong-Seok Chang* and Dewey H. Hodges†
Georgia Institute of Technology, Atlanta, Georgia 30332-1510

DOI: 10.2514/1.30733

Fundamental modeling of a flexible aircraft with a flying wing configuration, attached to a system of bungee cords, was developed in previous work of the authors. Herein this work is extended to include the capability of modeling a general configuration that can be represented as a collection of nonlinear beam finite elements. This allows one to model configurations with fuselage(s) and tail(s) in terms of beam finite elements. The finite element formulation is based on the fully intrinsic beam formulation, so that multiple beams are included by enforcing appropriate continuity conditions on velocity and angular velocity at nodes where beams intersect. Geometric constraints imposed by bungee cords attached at different points along a structure modeled with these beam elements make the system statically indeterminate. This brings certain strain-displacement relations and displacement variables into the formulation. Two in-depth parametric studies on how ground-vibration testing parameters affect the modal characteristics of highly flexible aircraft are presented as follows: 1) the effect of different bungee cord locations and 2) the effect of a fuselage structure on the modal characteristics. A comparison of results from the parametric studies provides information on how the shape of a highly flexible wing affects its modal characteristics and which eigenmodes associated with fuselage motion are involved in the low-frequency structural modes. In addition, for conventional configurations with highly flexible wings, the existence of modes identified in ground-vibration testing as predominantly rigid-body motion is discussed. Moreover, when such modes do exist, the extent to which they involve structural deformation and the effect of ground-vibration testing parameters on them is studied.

Nomenclature

Bungee Formulation

B	=	reference point of rigid body
$\mathbf{B}_i$	=	unit basis vector of body fixed reference frame
B^*	=	center of mass of rigid body
C	=	rotation matrix from inertial frame to body reference frame
F_k	=	Lagrange multiplier interpreted as tension of kth bungee cord
g	=	acceleration of gravity
K	=	kinetic energy
K_k	=	stiffness of kth bungee cord
ℓ_k	=	natural length of kth bungee cord
m	=	mass of rigid body
$\mathbf{n}_i$	=	unit basis vector of inertial frame
O	=	origin of the inertial frame
P	=	potential energy
P_k	=	point in rigid body attached to kth bungee cord
$\mathbf{P}_{OB^*}$	=	position vector from O to B^*
Q_k	=	point in inertial frame attached to kth bungee cord
x_B	=	$\mathbf{x} \cdot \mathbf{B}_i$ matrix components in body fixed reference frame basis
x_n	=	$\mathbf{x} \cdot \mathbf{n}_i$ matrix components in inertial basis
Δ	=	identity matrix
δ	=	variational operator
$\overline{\delta A}$	=	virtual action
$\overline{\delta q}$	=	virtual displacement
$\overline{\delta W}$	=	virtual work
$\overline{\delta \psi}$	=	virtual rotation
ϵ_k	=	slack variable for kth bungee cord
μ_k	=	Lagrange multiplier to enforce the unit vector condition for each $\boldsymbol{\tau}_k$
$\boldsymbol{\xi}$	=	position vector from B^* to arbitrary point in the body
σ_k	=	stretch of kth bungee cord
$\boldsymbol{\tau}_k$	=	unit vector along kth bungee cord

Multiple-Beam Formulation

B	=	deformed beam reference frame (B frame)
C^{iB}	=	rotation matrix from B frame to i
F	=	internal force measures in B frame
g	=	measure numbers of gravity vector in B frame
H	=	angular momentum measures
i	=	inertial frame
M	=	internal moment measures in B frame
P	=	linear momentum measures
V	=	velocity measures in B frame
$\hat{x}$	=	nodal variables
$\bar{x}$	=	element variables
$\overline{\gamma}$	=	internal strain measures
$\overline{\delta u}$	=	virtual displacement
$\overline{\delta \psi}$	=	virtual rotation
κ	=	internal curvature measures
Ω	=	angular velocity measures in B frame

Received 28 February 2007; accepted for publication 5 June 2007.

*Postdoctoral Fellow, School of Aerospace Engineering. Member AIAA.
†Professor, School of Aerospace Engineering. Fellow AIAA.

I. Introduction

WITH the advent of highly flexible aircraft, the results of ground-vibration testing (GVT) should be understood afresh in light of how those results apply to the aeroelastic behavior of such aircraft, because the shape of the vehicle in a trimmed flight condition might be very different from that of a GVT configuration suspended from bungee cords. Van Schoor and von Flotow [1] noticed the large

tip deflection of the wing in flight when they developed the human-powered aircraft Michelob Light Eagle. Therefore, the wing bending stiffness was modified, and wires were attached to each wing, so that the deformed shape of the flexible wing in GVT would match that of the wing in a 1 g trimmed flight condition as closely as possible.

In a usual GVT, a bungee cord or a soft supporting (airbag) system [2] is attached or located close to the center of mass. This choice will lead to a wing deflection opposite to that of the in-flight shape configuration for highly flexible aircraft due to gravity. A current lack of understanding raises new questions about how the GVT process should be conducted for highly flexible aircraft with high-aspect-ratio wings.

For the type of GVT under consideration in this paper, the vehicle is modeled by a collection of geometrically exact, nonlinear intrinsic beams [3–5] suspended from bungee cords. Here the term "intrinsic" refers to the special characteristic of a formulation to be without displacement and rotation variables.

Suspension of the model using bungee cords inevitably introduces a small amount of elastic deformation into the modes that would be the rigid-body modes of an unrestrained vehicle. These new modes we refer to as "GVT rigid-body modes" to distinguish them from true rigid-body modes. Previous work [6] showed that, to widely separate the frequencies of GVT rigid-body modes from those of the lowest-frequency elastic modes in a highly flexible aircraft restrained by linearly elastic bungee cords, the cords should be carefully positioned and their stiffnesses chosen sufficiently low. Consequently, these low stiffnesses can result in large elongation of the bungee cords.

Although the main interest of the present study is not the nonlinear dynamic analysis of the bungee cords per se, the nonlinear dynamic behavior of the GVT bungee system needs to be described properly for large elongation. Various mathematical stress–strain relations and strain energy functions have been proposed to improve correlation with experimental data in the range of large elongation. One approach depends on materials [7] and a piecewise linear approximation in the range of 2–250% elongation [8]. Another approach is to express the strain energy function in terms of an infinite series of strain invariants [9,10]. Finally, Arruda and Boyce [11] expressed the final form of strain energy function in terms of strain invariants with additional parameters such as chain density, Boltzmann's constant, and temperature.

In addition to a linear bungee model, the current analysis is based on the Hencky strain energy function, which has showed good accuracy for moderate deformation of several real materials [12] and good agreement with experimental data for large axial elongation [13]. Besides the bungee system, especially for large flexible space structures, a zero-spring-suspension system [14–16] can be used to make a sufficiently low bungee stiffness available. It provides negative stiffness to compensate for the stiffness associated with the suspension system, which is attached to the structure, by adapting proper mechanisms under a prestressed load.

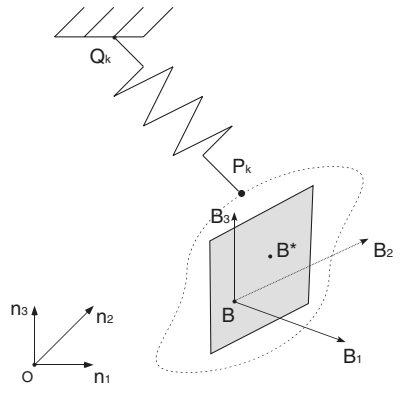

Fig. 1 Schematic of a bungee connection to a finite element node.

II. Bungee Formulation

In this section a formulation for a nonlinear bungee system is presented, with the bungee elongation described in terms of the Hencky strain energy [12,13] along with the previous linear model [6]. Figure 1 shows the schematic of a bungee connection to a finite element node. Consider a node attached to a support Q_k by a bungee cord. The point O is the origin of the inertial frame and $\mathbf{n}_i$ is an inertial frame basis unit vector. The point B^* is the center of mass of the rigid body, and the point B is the origin of the reference frame with the unit basis vector $\mathbf{B}_i$. The point P_k is taken to be the kth point in a rigid body attached to a bungee cord.

The linear bungee formulation in the previous work [6] is given for $k = 1, 2, \ldots, N$ as

$$\begin{aligned}
&K_k\sigma_k - F_k = 0\\
&-F_k(p_{OQ_k} - p_{OB^*} - C^T p_{B^*P_k}) + 2\mu_k\tau_{k_n} = 0\\
&\epsilon_k F_k = 0\\
&\ell_k + \sigma_k - \epsilon_k^2 + \tau_{k_n}^T(p_{OQ_k} - p_{OB^*} - C^T p_{B^*P_k}) = 0\\
&\tau_{k_n}^T\tau_{k_n} - 1 = 0\\
&\sigma_k - \zeta_k^2 = 0
\end{aligned} \tag{1}$$

where the subindex k is for the kth bungee cord, K_k is the stiffness of the kth bungee cord, σ_k is the deflection, F_k and μ_k are the Lagrange multipliers, ϵ_k is the slack variable, ℓ_k is the natural length of the bungee cord, $\boldsymbol{\tau}_k$ is a unit vector along the taut cord, $p_{OQ_{k_i}} = \mathbf{P}_{OQ_k}\cdot\mathbf{n}_i$, $p_{OB_i^*} = \mathbf{P}_{OB^*}\cdot\mathbf{n}_i$, $p_{B^*P_{k_i}} = \mathbf{P}_{B^*P_k}\cdot\mathbf{B}_i$, and $\tau_{k_{n_i}} = \boldsymbol{\tau}_k\cdot\mathbf{n}_i$.

In Eqs. (1), the third, fourth, and sixth equations are related to the slack conditions. The sixth equation is an additional equation for the slack condition of bungee cords. When a simple spring model is needed, slack variable ϵ_k along with the third and sixth equations can be eliminated from the bungee formulation. When compared to the resulting governing equations in previous work [17,18], the one derived in the present analysis section has a much simpler compact matrix form to avoid unnecessarily long algebraic geometric relations and thereby ease numerical computations.

To replace the previously developed linear bungee model with a nonlinear model, the corresponding potential energy is modified, replacing the usual quadratic term in the stretch with the Hencky strain energy [12,13], given by

$$P_{\text{Hencky}} = \sum_{k=1}^{N}\frac{1}{2}K_k\ell_k^2\left[\ell_n\left(1+\frac{\sigma_k}{\ell_k}\right)\right]^2 \tag{2}$$

This yields a nonlinear bungee formulation, which is summarized as

$$\begin{aligned}
&K_k\ell_k\frac{\ell_n(1+\sigma_k/\ell_k)}{1+\sigma_k/\ell_k} - F_k = 0\\
&-F_k(p_{OQ_k} - p_{OB^*} - C^T p_{B^*P_k}) + 2\mu_k\tau_{k_n} = 0\\
&\epsilon_k F_k = 0\\
&\ell_k + \sigma_k - \epsilon_k^2 + \tau_{k_n}^T(p_{OQ_k} - p_{OB^*} - C^T p_{B^*P_k}) = 0\\
&\tau_{k_n}^T\tau_{k_n} - 1 = 0\\
&\sigma_k - \zeta_k^2 = 0
\end{aligned} \tag{3}$$

Thus, only the first of Eqs. (1) is modified to produce the nonlinear analysis.

III. GVT in Multiple-Beam Configuration

GVT for conventional aircraft can be modeled by extending the fully intrinsic beam formulation [4] to treat structures made up of multiple beams, henceforth referred to as the "multiple-beam formulation." Figure 2 represents conventional aircraft in GVT as a multiple-beam structure. Both tips of beam 1 are attached to bungee cords, and the connection point between beams 2 and 3 is also attached to a bungee cord.

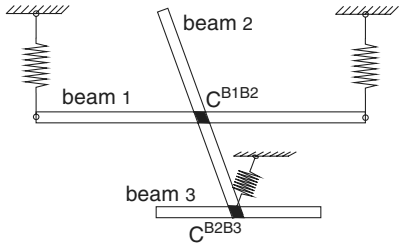

Fig. 2 Schematic of a conventional aircraft GVT, modeled as a multiple-beam structure restrained by bungee cords.

What follows is a brief description of how the fully intrinsic beam formulation [4,5] can be modified to treat a multiple-beam configuration. In Fig. 2, beams 1 and 2 share a node, and beams 2 and 3 share a node. Virtual displacements and rotations at the common nodes where beams intersect are not independent, thus yielding relations between virtual displacement and rotational variables in both beams such that

$$\overline{\delta u}_{\text{beam1}} = C^{B_1B_2}\overline{\delta u}_{\text{beam2}} \qquad \overline{\delta\psi}_{\text{beam1}} = C^{B_1B_2}\overline{\delta\psi}_{\text{beam2}} \tag{4}$$

where $C^{B_1B_2}$ is the rotation matrix from B_2 (reference frame of beam 2) to B_1 (reference frame of beam 1).

The separate nodal equations at the common node will be summed up as one set of nodal equations by the relation of the virtual displacement and rotation ($\overline{\delta u}_{\text{beam1,2}}$ and $\overline{\delta\psi}_{\text{beam1,2}}$) given in Eqs. (4). (This is a direct consequence of the derivations in [3–5], in which a detailed description of the nonlinear intrinsic formulation can be found.) As separate beams, the nodal equations regarding beam 1 are

$$\begin{aligned}
&\hat{F}^n_r - \hat{C}^{n^T}_{lr}\hat{F}^n_l + \hat{\mu}^n\hat{g}^n_r + \hat{f}^n - \dot{\hat{P}}^n_r - \tilde{\hat{\Omega}}^n_r\hat{P}^n_r = 0\\
&\hat{M}^n_r - \hat{C}^{n^T}_{lr}\hat{M}^n_l + \hat{m}^n_T + \hat{\mu}^n\tilde{\hat{\xi}}^n\hat{g}^n_r + \hat{m}^n - \dot{\hat{H}}^n_r - \tilde{\hat{\Omega}}^n_r\hat{H}^n_r - \tilde{\hat{V}}^n_r\hat{P}^n_r = 0
\end{aligned} \tag{5}$$

For beam 2, they are

$$\begin{aligned}
&\hat{F}^m_b - \hat{C}^{m^T}_{fb}\hat{F}^m_f + \hat{\mu}^m\hat{g}^m_b + \hat{f}^m - \dot{\hat{P}}^m_b - \tilde{\hat{\Omega}}^m_b\hat{P}^m_b = 0\\
&\hat{M}^m_b - \hat{C}^{m^T}_{fb}\hat{M}^m_f + \hat{m}^m_T + \hat{\mu}^m\tilde{\hat{\xi}}^m\hat{g}^m_b + \hat{m}^m - \dot{\hat{H}}^m_b\\
&\quad - \tilde{\hat{\Omega}}^m_b\hat{H}^m_b - \tilde{\hat{V}}^m_b\hat{P}^m_b = 0
\end{aligned} \tag{6}$$

At the common node these will reduce the separate nodal equations as follows:

$$\begin{aligned}
&\hat{F}^n_r - \hat{C}^{n^T}_{lr}\hat{F}^n_l + \hat{\mu}^n\hat{g}_r + \hat{f}^n - \dot{\hat{P}}^n_r - \tilde{\hat{\Omega}}^n_r\hat{P}^n_r\\
&\quad + C^{B_1B_2}(\hat{F}^m_b - \hat{C}^{m^T}_{fb}\hat{F}^m_f) = 0\\
&\hat{M}^n_r - \hat{C}^{n^T}_{lr}\hat{M}^n_l + \hat{\mu}^n\tilde{\hat{\xi}}^n\hat{g}_r + \hat{m}^n - \dot{\hat{H}}^n_r - \tilde{\hat{\Omega}}^n_r\hat{H}^n_r\\
&\quad - \tilde{\hat{V}}^n_r\hat{P}^n_r + C^{B_1B_2}(\hat{M}^m_b - \hat{C}^{m^T}_{fb}\hat{M}^m_f) = 0
\end{aligned} \tag{7}$$

In Eqs. (7), several terms such as $\hat{\mu}^m\hat{g}^m_b$, $\hat{f}^m$, $\hat{P}^m_b$, $\hat{m}^m_T$, $\hat{\mu}^m\tilde{\hat{\xi}}^m\hat{g}^m_b$, $\hat{m}^m$, and $\hat{H}^m_b$ in beam 2 are dropped from the separate nodal equation because those become redundant if beam 1 is taken as the master and beam 2 is relegated to slave status at the common node. The resulting equations count as only one set of governing equations, and the process leads to a loss of six nodal equations. These lost equations are compensated by the continuity conditions at the common node, viz.,

$$\hat{V}_{\text{beam1}} = C^{B_1B_2}\hat{V}_{\text{beam2}} \qquad \hat{\Omega}_{\text{beam1}} = C^{B_1B_2}\hat{\Omega}_{\text{beam2}} \tag{8}$$

Moreover, the boundary conditions for the gravity vector at the common node are given by

$$\hat{g}_{\text{beam1}} = C^{B_1B_2}\hat{g}_{\text{beam2}} \tag{9}$$

Finally, Eqs. (7–9) are new types of nodal equations if beams intersect. And these equations are also involved in the eigenanalysis for the linearized dynamics about the nonlinear static equilibrium state. Moreover, to determine a static equilibrium, Eqs. (7–9) are also used, dropping all the dynamic terms such as $\hat{\Omega}^n_r$, $\hat{V}^n_r$, $\dot{\hat{P}}^n_r$, and $\dot{\hat{H}}^n_r$. But Eqs. (8) are not necessary because $\hat{V}$ and $\hat{\Omega}$ become zero at static equilibrium and thus need not be included as variables.

Additionally, the strain-displacement relation is needed to relate the locations of bungee cords attached to beams 1 and 2. First, the attachment point for one of the three bungee cords is chosen as a reference. Then, one may integrate the strain-displacement relations to obtain locations of the other bungee cords. For example, if the attachment point at the left tip of beam 1 is taken as the reference shown in Fig. 2, two sets of strain-displacement relations are required: one from the reference point to the right tip of beam 1 and another from the reference point to the tail end of beam 2.

IV. Final GVT Formulation in Multiple-Beam Configuration

The element equations of the intrinsic beam formulation are

$$\begin{aligned}
&\frac{\hat{F}^{n+1}_l - \hat{F}^n_r}{dl} + (\tilde{\bar{\kappa}}^n + \tilde{\bar{k}}^n)\bar{F}^n + \mu^n\bar{g}^n - \dot{\bar{P}}^n - \tilde{\bar{\Omega}}^n\bar{P}^n = 0\\
&\frac{\hat{M}^{n+1}_l - \hat{M}^n_r}{dl} + (\tilde{\bar{\kappa}}^n + \tilde{\bar{k}}^n)\bar{M}^n + (\tilde{e}_1 + \tilde{\bar{\gamma}}^n)\bar{F}^n + \mu^n\tilde{\bar{\xi}}^n\bar{g}^n - \dot{\bar{H}}^n\\
&\quad - \tilde{\bar{\Omega}}^n\bar{H}^n - \tilde{\bar{V}}^n\bar{P}^n = 0\\
&\frac{\hat{V}^{n+1}_l - \hat{V}^n_r}{dl} + (\tilde{\bar{\kappa}}^n + \tilde{\bar{k}}^n)\bar{V}^n + (\tilde{e}_1 + \tilde{\bar{\gamma}}^n)\bar{\Omega}^n - \dot{\bar{\gamma}}^n = 0\\
&\frac{\hat{\Omega}^{n+1}_l - \hat{\Omega}^n_r}{dl} + (\tilde{\bar{\kappa}}^n + \tilde{\bar{k}}^n)\bar{\Omega}^n - \dot{\bar{\kappa}}^n = 0\\
&\frac{\hat{g}^{n+1}_l - \hat{g}^n_r}{dl} + (\tilde{\bar{\kappa}}^n + \tilde{\bar{k}}^n)\bar{g}^n = 0
\end{aligned} \tag{10}$$

These nodal equations are modified as follows if the node is attached to a bungee cord (case 1) or the node is a common node (case 2):

$$\begin{aligned}
&\hat{F}^n_r - \hat{C}^{n^T}_{lr}\hat{F}^n_l + \hat{\mu}^n\hat{g}^n_r + \hat{f}^n - \dot{\hat{P}}^n_r - \tilde{\hat{\Omega}}^n_r\hat{P}^n_r - F_k\tau_{k_B}\\
&\quad = 0 \quad \leftarrow \text{case 1}\\
&\hat{F}^n_r - \hat{C}^{n^T}_{lr}\hat{F}^n_l + \hat{\mu}^n\hat{g}^n_r + \hat{f}^n - \dot{\hat{P}}^n_r - \tilde{\hat{\Omega}}^n_r\hat{P}^n_r + C^{B_1B_2}(\hat{F}^m_b - \hat{C}^{m^T}_{fb}\hat{F}^m_f)\\
&\quad = 0 \quad \leftarrow \text{case 2}
\end{aligned} \tag{11}$$

$$\begin{aligned}
&\hat{M}^n_r - \hat{C}^{n^T}_{lr}\hat{M}^n_l + \hat{\mu}^n\tilde{\hat{\xi}}^n\hat{g}^n_r + \hat{m}^n - \dot{\hat{H}}^n_r - \tilde{\hat{\Omega}}^n_r\hat{H}^n_r - \tilde{\hat{V}}^n_r\hat{P}^n_r\\
&\quad - \tilde{p}_{BP_k}(F_k\tau_{k_B}) = 0 \quad \leftarrow \text{case 1}\\
&\hat{M}^n_r - \hat{C}^{n^T}_{lr}\hat{M}^n_l + \hat{\mu}^n\tilde{\hat{\xi}}^n\hat{g}^n_r + \hat{m}^n - \dot{\hat{H}}^n_r - \tilde{\hat{\Omega}}^n_r\hat{H}^n_r - \tilde{\hat{V}}^n_r\hat{P}^n_r\\
&\quad + C^{B_1B_2}(\hat{M}^m_b - \hat{C}^{m^T}_{fb}\hat{M}^m_f) = 0 \quad \leftarrow \text{case 2}
\end{aligned}$$

The variables $\hat{V}_r$ and $\hat{\Omega}_r$ of the beam formulation are related to the position of a rigid body mounted at a node by kinematical relations

$$V_B = \dot{p}_{OB} + \tilde{\Omega}_B p_{OB} = \hat{V}^{(m)}_r \qquad \tilde{\Omega}_B = -\dot{C}_m C^T_m = \tilde{\hat{\Omega}}^{(m)}_r \tag{12}$$

Additionally, six conditions from $C^TC = \Delta$ are required to determine the orientation of the rigid body because no parameterization of rotation is introduced; thus, C has 3 degrees of freedom.

The strain-displacement relation is

$$C^T_{m+1}p_{OB^*_{m+1}} = C^T_m p_{OB^*_m} + \sum_{j=1}^{J}\bar{C}^{iB^j}(\bar{\gamma}^j + e_1)dl^j \tag{13}$$

and the relations to connect the orientation are expressed as

$$\hat{C}^{Bi^{n+1}} C_{m+1}^T = \Delta \tag{14}$$

$$\hat{g}_r^m = C_m \lfloor 0 \;\; 0 \;\; -1 \rfloor^T \tag{15}$$

For each bungee cord ($k = 1, 2, \ldots$)

$$\begin{aligned}
&K_k \ell_k \frac{\ell_n(1+\sigma_k/\ell_k)}{1+\sigma_k/\ell_k} - F_k = 0 \\
&-F_k(p_{OQ_k} - p_{OB} - C^T p_{BP_k}) + 2\mu_k \tau_{k_n} = 0 \\
&\epsilon_k F_k = 0 \\
&\ell_k + \sigma_k - \epsilon_k^2 + \tau_{k_n}^T (p_{OQ_k} - p_{OB} - C^T p_{BP_k}) = 0 \\
&\tau_{k_n}^T \tau_{k_n} - 1 = 0 \\
&\sigma_k - \zeta_k^2 = 0
\end{aligned} \tag{16}$$

The 12 boundary conditions, which are $\hat{F}_l^1 = \hat{F}_r^{N+1} = \hat{M}_l^1 = \hat{M}_r^{N+1} = 0$, complete the dynamic formulation.

V. Linearization for Eigenanalysis

For eigenanalysis, the set of governing equations derived in the previous section is linearized about a static equilibrium state. Let X be each state variable:

$$X = X_{\text{eq}} + X^*(t) \tag{17}$$

where X_{eq} is the value at static equilibrium, and $X^*(t)$ is the small perturbation on each state.

So a small perturbation on each variable can be expressed as

$$\begin{aligned}
&p_{OB^*} = p_{OB^*_{\text{eq}}} + u^* \\
&V_B = V_{B_{\text{eq}}} + V_B^* = V_B^* \\
&C = C_{\text{eq}} + C^* = (\Delta - \tilde{\theta}^*) C_{\text{eq}} \\
&\Omega = \Omega_{\text{eq}} + \Omega^* = \Omega^* \\
&F_k = F_{k_{\text{eq}}} + F_k^* \\
&\tau_{k_B} = \tau_{k_{B_{\text{eq}}}} + \tau_{k_B}^* \\
&\sigma_k = \sigma_{k_{\text{eq}}} + \sigma_k^* \\
&\mu_k = \mu_{k_{\text{eq}}} + \mu_k^* \\
&\epsilon_k = \epsilon_{k_{\text{eq}}} + \epsilon_k^* \\
&\zeta_k = \zeta_{k_{\text{eq}}} + \zeta_k^*
\end{aligned} \tag{18}$$

The linearized element equations from the intrinsic beam formulation are

$$\begin{aligned}
&\frac{\hat{F}_l^{*n+1} - \hat{F}_r^{*n}}{dl} + (\tilde{\bar{\kappa}}_{\text{eq}}^n + \tilde{\bar{k}}^n)\bar{F}^{*n} + \tilde{\bar{\kappa}}^{*n} \bar{F}_{\text{eq}}^n + \mu^n \bar{g}^{*n} = \dot{\bar{P}}^{*n} \\
&\frac{\hat{M}_l^{*n+1} - \hat{M}_r^{*n}}{dl} + (\tilde{\bar{\kappa}}_{\text{eq}}^n + \tilde{\bar{k}}^n)\bar{M}^{*n} + \tilde{\bar{\kappa}}^{*n} \bar{M}_{\text{eq}}^n + (\tilde{e}_1 + \tilde{\bar{\gamma}}_{\text{eq}}^n)\bar{F}^{*n} \\
&\quad + \tilde{\bar{\gamma}}^{*n} \bar{F}_{\text{eq}}^n + \mu^n \tilde{\bar{\xi}}^n \bar{g}^{*n} = \dot{\bar{H}}^{*n} \\
&\frac{\hat{V}_l^{*n+1} - \hat{V}_r^{*n}}{dl} + (\tilde{\bar{\kappa}}_{\text{eq}}^n + \tilde{\bar{k}}^n)\bar{V}^{*n} + (\tilde{e}_1 + \tilde{\bar{\gamma}}_{\text{eq}}^n)\bar{\Omega}^{*n} = \dot{\bar{\gamma}}^{*n} \\
&\frac{\hat{\Omega}_l^{*n+1} - \hat{\Omega}_r^{*n}}{dl} + (\tilde{\bar{\kappa}}_{\text{eq}}^n + \tilde{\bar{k}}^n)\bar{\Omega}^{*n} = \dot{\bar{\kappa}}^{*n} \\
&\frac{\hat{g}_l^{*n+1} - \hat{g}_r^{*n}}{dl} + (\tilde{\bar{\kappa}}_{\text{eq}}^n + \tilde{\bar{k}}^n)\bar{g}^{*n} + \tilde{\bar{\kappa}}^{*n} \bar{g}_{\text{eq}}^n = 0
\end{aligned} \tag{19}$$

The nodal equations with the modifications for case 1 (for which the node is attached to the bungee cord) and for case 2 (for which the node is a common node) are linearized as follows:

$$\begin{aligned}
&\hat{F}_r^{*n} - \hat{C}_{lr}^{n^T} \hat{F}_l^{*n} + \hat{\mu}^n \hat{g}_r^{*n} + \hat{f}^{*n} - \dot{\hat{P}}_r^{*n} - F_{k_{\text{eq}}} \tau_{k_B}^* - F_k^* \tau_{k_{B_{\text{eq}}}} \\
&\quad = 0 \quad \leftarrow \text{case 1} \\
&\hat{F}_r^{*n} - \hat{C}_{lr}^{n^T} \hat{F}_l^{*n} + \hat{\mu}^n \hat{g}_r^{*n} + \hat{f}^{*n} - \dot{\hat{P}}_r^{*n} + C^{B_1 B_2} (\hat{F}_b^{*m} - \hat{C}_{fb}^{m^T} \hat{F}_f^{*m}) \\
&\quad = 0 \quad \leftarrow \text{case 2}
\end{aligned} \tag{20}$$

$$\begin{aligned}
&\hat{M}_r^{*n} - \hat{C}_{lr}^{n^T} \hat{M}_l^{*n} + \hat{\mu}^n \tilde{\hat{\xi}}^n \hat{g}_r^{*n} + \hat{m}^{*n} - \dot{\hat{H}}_r^{*n} \\
&\quad - \tilde{p}_{BP_k} (F_{k_{\text{eq}}} \tau_{k_B}^* + F_k^* \tau_{k_{B_{\text{eq}}}}) = 0 \quad \leftarrow \text{case 1} \\
&\hat{M}_r^{*n} - \hat{C}_{lr}^{n^T} \hat{M}_l^{*n} + \hat{\mu}^n \tilde{\hat{\xi}}^n \hat{g}_r^{*n} + \hat{m}^{*n} - \dot{\hat{H}}_r^{*n} \\
&\quad + C^{B_1 B_2} (\hat{M}_b^{*m} - \hat{C}_{fb}^{*m^T} \hat{M}_f^m) = 0 \quad \leftarrow \text{case 2}
\end{aligned}$$

The linearized continuity conditions for a multiple-beam structure are

$$\begin{aligned}
&\hat{V}^*_{\text{beam1}} = C^{B_1 B_2} \hat{V}^*_{\text{beam2}} \qquad \hat{\Omega}^*_{\text{beam1}} = C^{B_1 B_2} \hat{\Omega}^*_{\text{beam2}} \\
&\hat{g}^*_{\text{beam1}} = C^{B_1 B_2} \hat{g}^*_{\text{beam2}}
\end{aligned} \tag{21}$$

The linearized kinematical relations at the nodes to which bungee cords are attached are

$$\hat{V}_r^{*m} = \dot{u}^* + \tilde{\Omega}_r^{*m} p_{OB_{\text{eq}}}^m \tag{22}$$

and

$$\tilde{\Omega}_r^{*m} = \tilde{\dot{\theta}}^{*m} \tag{23}$$

One difficulty arises in the linearization of the additional equations for GVT modeling, namely, the set of relations between strain and displacement/rotation variables. It is infeasible to get an analytic expression for the linearized version of Eq. (13), and the three independent choices $A_{11} = 1, A_{12} = 0, A_{23} = 0$ from Eqs. (14) where $A_{ij} = (\hat{C}^{Bi^{n+1}} C_{m+1}^T)_{ij}$. So the one from a numerical perturbation of these equations with respect to each state is substituted for the analytic counterpart, viz.,

$$B_{\text{num}} = \frac{F_{\text{num}}(X_{\text{eq}} + q) - F_{\text{num}}(X_{\text{eq}} - q)}{2q} \tag{24}$$

where B_{num} is the Jacobian matrix, q is a numerical perturbation, and

$$F_{\text{num}} = \left\{ \begin{array}{c} C_{m+1}^T p_{OB^*_{m+1}} - C_m^T p_{OB^*_m} - \sum_{j=1}^J \bar{C}^{iB^j} (\bar{\gamma}^j + e_1) dl^j \\ A_{11} - 1 \\ A_{12} \\ A_{23} \end{array} \right\}_{6\times 1} \tag{25}$$

$$\hat{g}_r^{*m} = -\tilde{\theta}^* C_{\text{eq}}^m \lfloor 0 \;\; 0 \;\; -1 \rfloor^T \tag{26}$$

For each bungee cord ($k = 1, 2, \ldots,$),

$$\begin{aligned}
&K_k \frac{1 - \ell_n(1+\sigma_{k_{\text{eq}}}/\ell_k)}{(1+\sigma_{k_{\text{eq}}}/\ell_k)^2} \sigma_k^* - F_k^* = 0 \\
&-F_k^* (C_{\text{eq}} p_{OQ_k} - p_{OB^*_{\text{eq}}} - p_{B^* P_k}) + F_{k_{\text{eq}}} (u^* + \tilde{\theta}^* C_{\text{eq}} p_{OQ_k}) \\
&\quad + 2(\mu_{k_{\text{eq}}} \tau_{k_B}^* + \tau_{k_{B_{\text{eq}}}} \mu_k^*) = 0 \\
&\epsilon_{k_{\text{eq}}} F_k^* + F_{k_{\text{eq}}} \epsilon_k^* = 0 \\
&\sigma_k^* - 2\epsilon_{k_{\text{eq}}} \epsilon_k^* - \tau_{k_{B_{\text{eq}}}}^T (u^* + \tilde{\theta}^* C_{\text{eq}} p_{OQ_k}) \\
&\quad + (C_{\text{eq}} p_{OQ_k} - p_{OB^*_{\text{eq}}} - p_{B^* P_k})^T \tau_{k_B}^* = 0 \\
&\tau_{k_{B_{\text{eq}}}}^T \tau_{k_B}^* = 0 \qquad \sigma_k^* - 2\zeta_{k_{\text{eq}}} \zeta_k^* = 0
\end{aligned} \tag{27}$$

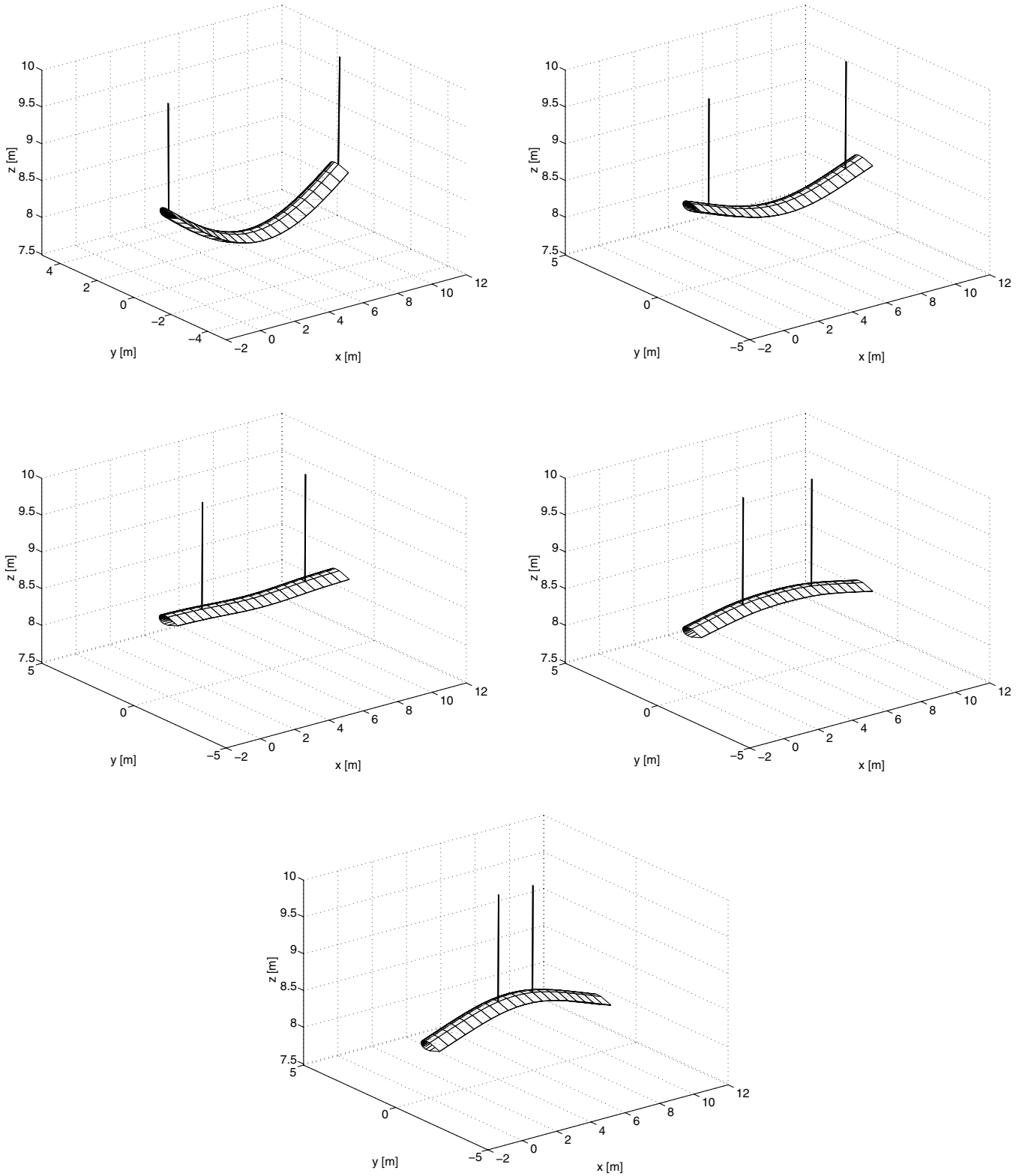

Fig. 3 Static equilibria of cases 1–5 (from top to bottom, from left to right, the case number increases as the bungee cord location moves to the midspan).

The 12 boundary conditions, which are $\hat{F}_l^{*1} = \hat{F}_r^{*N+1} = \hat{M}_l^{*1} = \hat{M}_r^{*N+1} = 0$, complete the system of linearized equations.

VI. Parametric Study

The developed formulation is applicable to configurations that can be represented as multiple beams. It is here applied to two configurations, which will serve as illustrative examples: flying wing configuration (FWC) and conventional aircraft configuration (CAC) with wings, fuselage, and tail.

A. Effect of Bungee Cord Locations on Modal Characteristics

Because the wing is highly flexible and loaded by its own weight, its deformed shape in GVT will differ according to the locations of points to which bungee cords are connected. The study looks at different bungee cord attachment points to observe differences in modal characteristics affected by the deformed shape of the flexible wing. Case 1 has the bungee cords attached to each tip of the flexible beam, and case 5 has them attached close to midspan. Cases 2–4 are intermediate cases between cases 1 and 5. The static equilibrium of each case is shown in Fig. 3 with the given properties in Table 1.

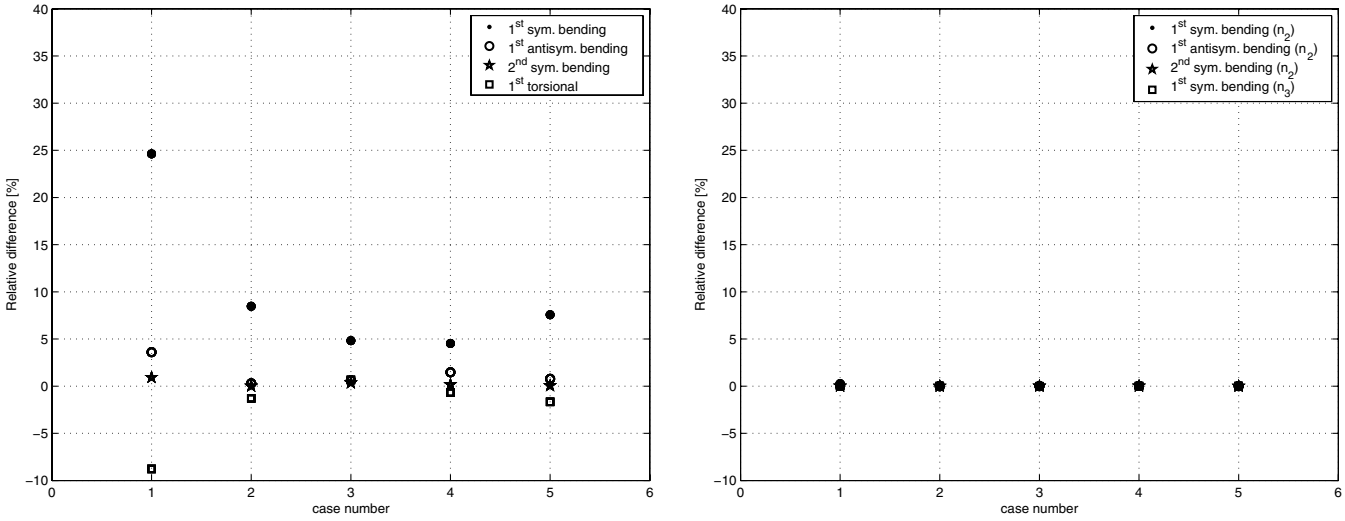

Fig. 4 Relative difference of four lowest elastic modes for cases 1–5 of flexible (left figure) and stiff (right figure) beams with respect to those of the free–free beam; the horizontal axis corresponds to the case number.

Depending on the locations of bungee cords, the deformed shapes of a highly flexible beam in GVT are very different. For example, cases 1, 3, and 5 show the configuration as a deformed U, approximately flat, and as an inverted U, respectively.

Table 1 Beam and bungee cord properties

	Property	Value		Unit
m	Mass per unit length	10		kg/m
ℓ	Total length of wing	10		m
$d\ell$	Element length	0.5		m
k	Bungee stiffness	2000		N/m
		Flexible	Stiff	
GJ	Torsional stiffness	1.0×10^4	1.0×10^6	Nm^2
EI_2	Vertical bending stiffness	2.0×10^4	2.0×10^6	Nm^2
EI_3	Chordwise bending stiffness	4.0×10^6	1.0×10^8	Nm^2

Table 2 shows the 10 lowest eigenmodes and their eigenvalues for flexible beam cases 1–5. Values for the four lowest eigenvalues of stiff beams are added for comparison. (n_2 and n_3 are flapwise and chordwise directions, respectively). The relative differences of the four lowest elastic modes of a flexible and a stiff beam for cases 1–5 with respect to those of the free–free boundary condition are shown in Fig. 4 in order to see the changes in the modal frequencies. The horizontal axis corresponds to the case numbers (i.e., 1 on the horizontal axis indicates case 1). The left figure of Fig. 4 clearly shows that the modal frequencies of the highly flexible beam are affected in GVT. The modal frequencies of the U shape (case 1) and inverted U shape (case 5) are most different from those of the free–free beam. The result also indicates that some of the structural modes such as first symmetric bending and first torsional modes are more influenced.

The main contributors that lead the differences between modal characteristics for cases 1–5 are both of the deformed shape, which is determined by the location of points to which bungee cords are

Table 2 Eigenvalues of cases 1–5 with the four lowest eigenvalues of flexible and stiff beams (rad/s)

Flexible beam Eigenmode	Case 1	Case 2	Case 3	Case 4	Case 5
(Lateral) swing	$\pm 2.2574i$	$\pm 2.4468i$	$\pm 2.5309i$	$\pm 1.8278i$	$\pm 0.9163i$
(Fore–aft) swing	$\pm 2.6316i$	$\pm 2.6313i$	$\pm 2.6312i$	$\pm 2.4791i$	$\pm 1.3353i$
Plunging	$\pm 2.9358i$	$\pm 3.3532i$	$\pm 2.7378i$	$\pm 2.5110i$	$\pm 2.4492i$
Twisting	$\pm 4.5561i$	$\pm 3.6493i$	$\pm 3.5888i$	$\pm 2.6593i$	$\pm 2.6425i$
Rolling	$\pm 6.0353i$	$\pm 5.0162i$	$\pm 3.7530i$	$\pm 3.5289i$	$\pm 3.3556i$
Pitching	$\pm 12.082i$	$\pm 10.823i$	$\pm 10.161i$	$\pm 10.339i$	$\pm 10.807i$
1st sym. bending, n_2	$\pm 12.582i$	$\pm 10.951i$	$\pm 10.583i$	$\pm 10.553i$	$\pm 10.860i$
1st antisym. bending, n_2	$\pm 29.326i$	$\pm 28.392i$	$\pm 28.480i$	$\pm 28.725i$	$\pm 28.526i$
2nd sym. bending, n_2	$\pm 57.444i$	$\pm 56.919i$	$\pm 57.115i$	$\pm 57.003i$	$\pm 56.944i$
1st torsional	$\pm 90.817i$	$\pm 98.260i$	$\pm 100.23i$	$\pm 98.872i$	$\pm 97.895i$
Stiff beam					
1st sym. bending, n_2	$\pm 101.23i$	$\pm 101.04i$	$\pm 100.97i$	$\pm 100.99i$	$\pm 101.04i$
1st antisym. bending, n_2	$\pm 283.17i$	$\pm 283.07i$	$\pm 283.08i$	$\pm 283.11i$	$\pm 283.09i$
2nd sym. bending, n_2	$\pm 569.20i$	$\pm 569.15i$	$\pm 569.16i$	$\pm 569.16i$	$\pm 569.15i$
1st sym. bending, n_3	$\pm 714.06i$	$\pm 713.96i$	$\pm 713.92i$	$\pm 713.93i$	$\pm 713.96i$

Table 3 Eigenvalues of cases 1, 3, and 5 with the low stiffness ($k = 20$ N/m), and of the free–free flexible beam (rad/s)

Eigenmode	Case 1	Case 3	Case 5	Free–free beam
1st sym. bending, n_2	$\pm 10.409i$	$\pm 10.195i$	$\pm 10.120i$	$\pm 10.096i$
1st antisym. bending, n_2	$\pm 28.382i$	$\pm 28.327i$	$\pm 28.309i$	$\pm 28.307i$
2nd sym. bending, n_2	$\pm 56.942i$	$\pm 56.912i$	$\pm 56.893i$	$\pm 56.915i$
1st torsional	$\pm 90.419i$	$\pm 100.19i$	$\pm 97.880i$	$\pm 99.551i$

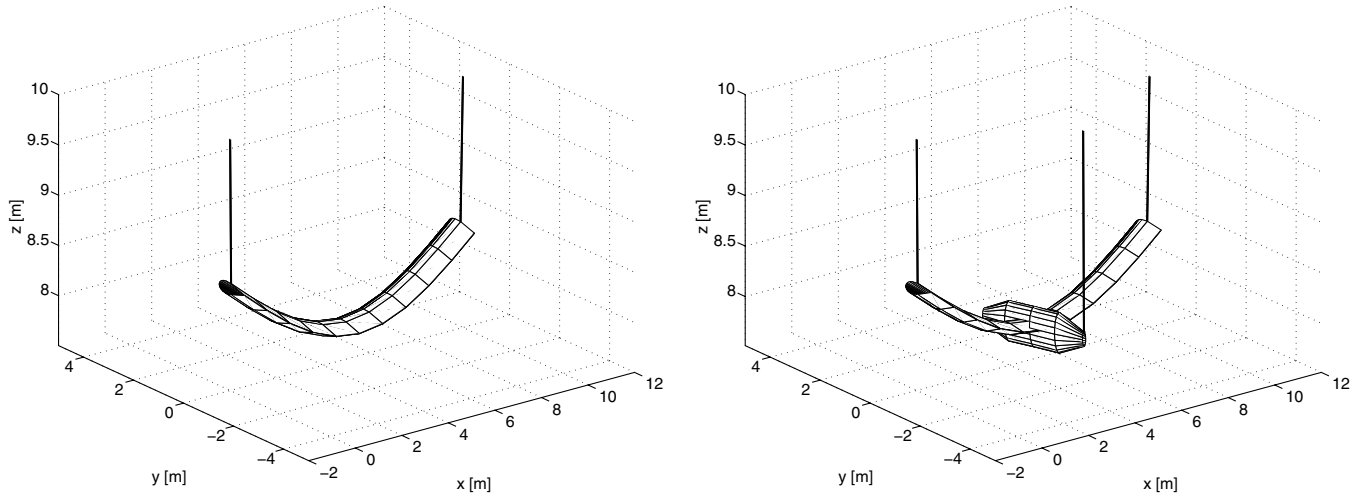

Fig. 5 3-D plot of GVT static equilibria of FWC and CAC.

attached, and a boundary condition due to bungee cords. To see only the effect of bungee cord locations, the bungee stiffness value should decrease to a low value because, as the bungee stiffness reduces, the analysis will nearly exclude the contribution of the bungee cords as a constraining boundary condition to the beam. Here, it reduces to $k = 20$ N/m from 2000 N/m. Cases 1, 3, and 5 (which are a deformed U, approximately flat, and an inverted U, respectively), are simulated with the low bungee stiffness ($k = 20$ N/m).

The results of low stiffness ($k = 20$ N/m) cases are given in Table 3. Some changes in the four lowest eigenvalues are observed

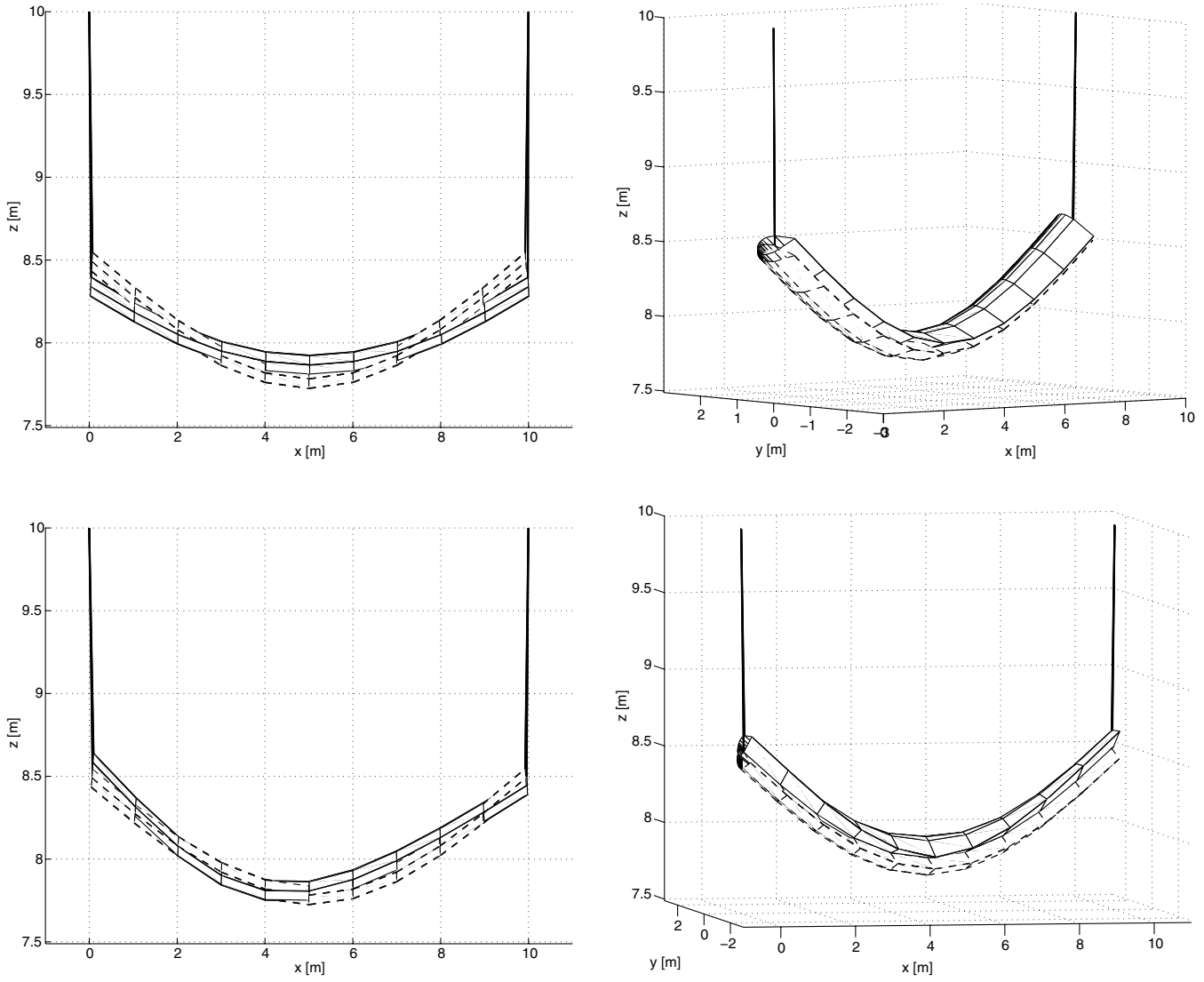

Fig. 6 First–fourth GVT structural mode shapes of FWC.

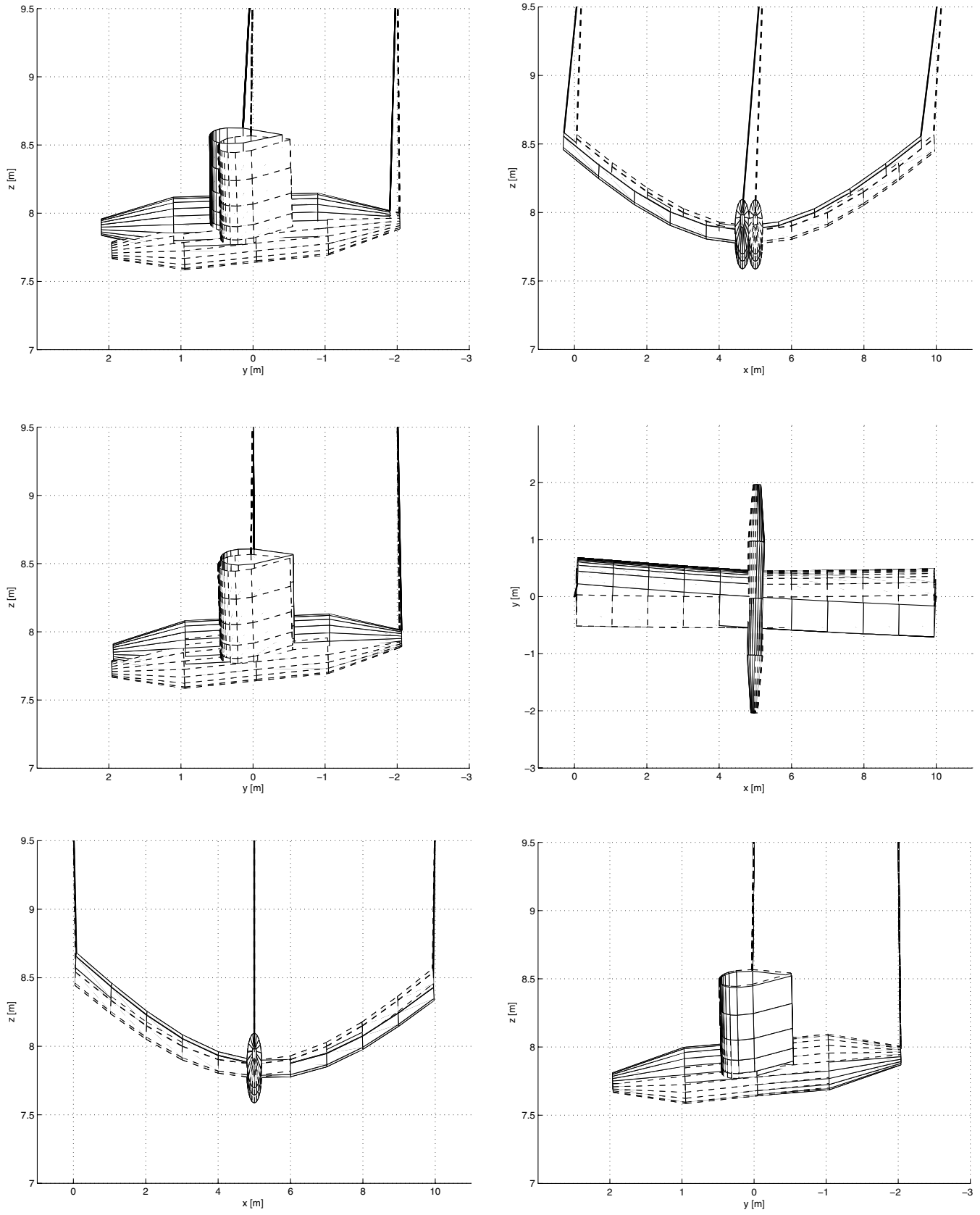

Fig. 7 First–sixth GVT rigid-body mode shapes of CAC.

through comparing Table 2 of $k = 2000$ N/m with Table 3 of $k = 20$ N/m, and these changes are directly related to the influence of bungee stiffness on the modal characteristics. First, the first symmetric bending eigenvalue in case 1 changes from $\pm 12.582i$ in Table 2 to $\pm 10.409i$ in Table 3, which indicates that if bungee cords are located at points where significant displacement occurs, the first symmetric bending eigenvalue will be greater than the corresponding first free–free beam symmetric bending eigenvalue ($\pm 10.096i$). The level of overestimation will depend on the bungee stiffness value. Second, the first torsional eigenvalue in cases 1 and 5 does not change much, from $\pm 90.817i$ to $\pm 90.419i$ and $\pm 97.895i$ to $\pm 97.880i$, respectively; and the eigenvalue for case 3 also does not change

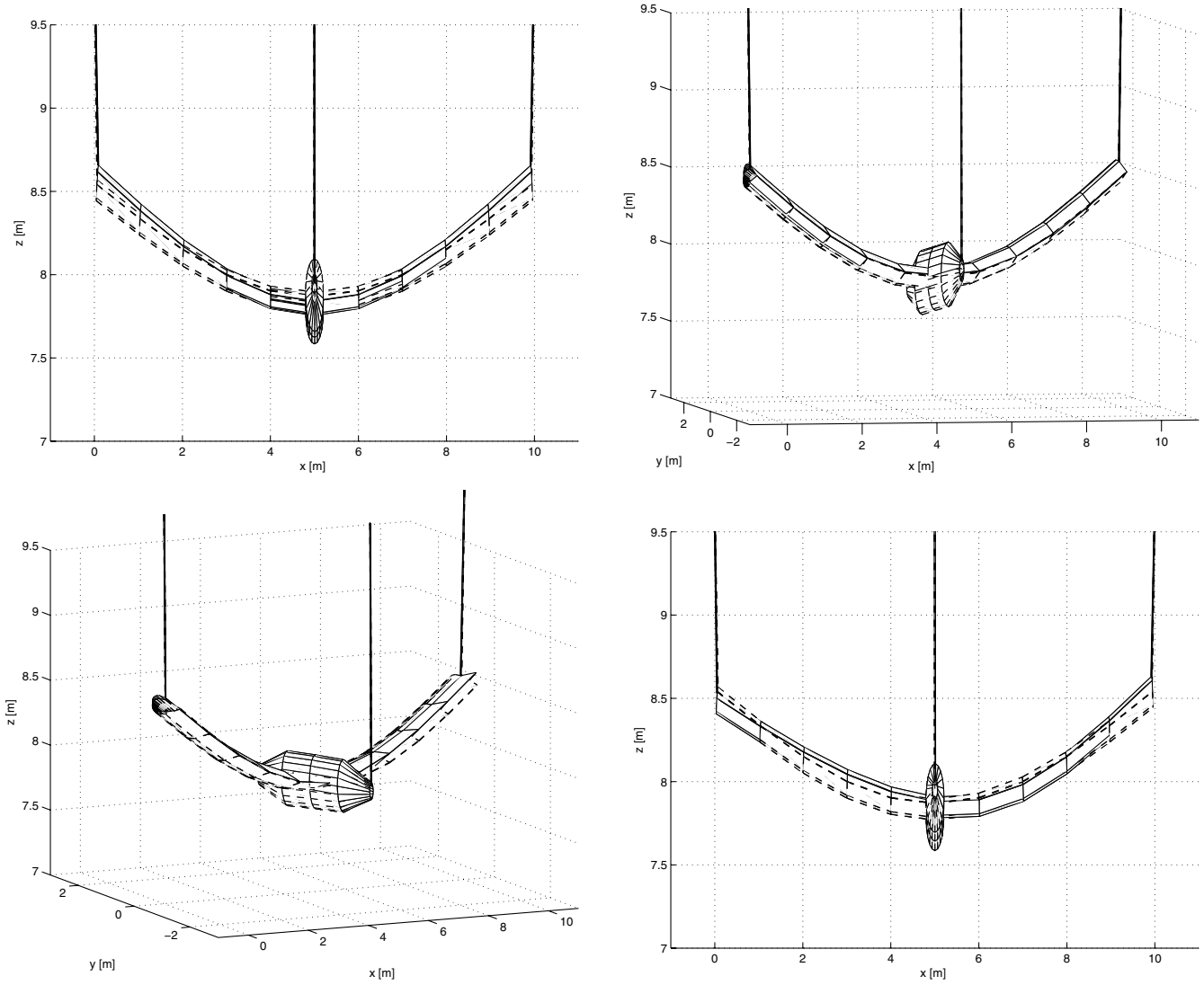

Fig. 8 First–fourth GVT structural mode shapes of CAC.

much, from $\pm 100.23i$ to $\pm 100.19i$. These results indicate that the first torsional mode is not significantly influenced by stiffness values of bungee cords because it does not contain significant amounts of either longitudinal or lateral deflection.

In Table 3, the relative differences of each eigenvalue to those of a free–free beam will only indicate the influence of the deformed shape on its modal characteristic. First, case 1, which deforms the most among the three cases, has the largest relative difference in first symmetric bending eigenvalue with respect to the free–free beam case. Second, the first torsional eigenvalue for case 3 ($\pm 100.19i$) is closest to the free–free solution ($\pm 99.551i$), which shows that the deformed U and inverted U shapes tend to lower the first torsional

Table 4 Beam and bungee cord properties

Property	Wing	Fuselage	Units
m: mass per unit length	7	7	kg/m
ℓ: total length	10	4	m
$d\ell$: element length	1	1	m
GJ: torsional stiffness	1.0×10^4	1.0×10^4	Nm^2
EI_2: vertical bending stiffness	2.0×10^4	2.0×10^4	Nm^2
EI_3: chordwise bending stiffness	4.0×10^6	4.0×10^6	Nm^2
	Bungees 1, 2	Bungee 3	
k: bungee stiffness	2000	1500	N/m
ℓ_b: bungee natural length	1	1.9	m

Table 5 Ten lowest GVT modes and corresponding eigenvalues of FWC

Eigenvalues, rad/s	Description
$0 \pm 2.1620i$	Swing mode (fore and aft) + plunging mode
$0 \pm 2.6468i$	Swing mode (lateral)
$0 \pm 2.8578i$	Plunging mode
$0 \pm 5.4405i$	Twisting mode
$0 \pm 7.1118i$	Pitching mode
$0 \pm 7.3779i$	Rolling mode
$0 \pm 13.589i$	1st symmetric bending mode (vertical)
$0 \pm 33.185i$	Torsional mode with 180 deg phase shift between right and left tips
$0 \pm 37.935i$	1st antisymmetric vertical bending mode
$0 \pm 49.569i$	Torsional mode with same phase between right and left tips (i.e., the torsional mode of the left wing is a mirror image of the right one)

Table 6 Ten lowest GVT modes and corresponding eigenvalues of CAC

Eigenvalues	Description
$\pm 2.3710i$	Swing mode (fore and aft)
$\pm 2.6261i$	Swing mode (lateral)
$\pm 3.3024i$	Pitching about tail
$\pm 5.1714i$	Twisting mode
$\pm 7.4294i$	Rolling mode
$\pm 11.896i$	Pitching mode
$\pm 14.298i$	1st symmetric wing bending mode (vertical)
$\pm 30.961i$	Wing torsional mode with same phase between right and left tips
$\pm 32.925i$	Wing torsional mode with 180 deg phase shift between right and left tips
$\pm 35.340i$	1st antisymmetric wing vertical bending mode

eigenvalue relative to the corresponding eigenvalue of the free–free beam.

Table 2 for the stiffer beam shows that the low structural modes are separated enough from the GVT rigid-body modes induced by the suspension system (i.e., bungee system), and the suspension system has an ignorable effect on the modal characteristics. In addition, the relative differences among the four lowest structural modal frequencies for each case are not very noticeable, as shown in the right part of Fig. 4 because the deformation in GVT is much smaller than for the more flexible beam.

B. Modal Characteristics Comparison of FWC and CAC in GVT

GVT modal characteristics for FWC and CAC configurations are compared while attempting to keep some of the properties as close to equivalent as possible. For the FWC, the payload is located at midspan, which corresponds to the total mass of fuselage for the CAC. The static equilibrium of each case is shown in Fig. 5 with the wing, fuselage, and bungee properties in Table 4. For simplicity the tail(s) of the CAC can be replaced by a concentrated mass at the tail end of the fuselage. Bungee cords 1 and 2 are attached to each wing tip, and bungee cord 3 is attached to the fuselage tip for the CAC.

The GVT analysis gives information about two distinctive types of modal characteristics. One is the GVT rigid-body modes (in which the beam remains almost rigid), and the other is structural modes of the flexible beam element. Usually, the GVT rigid-body modes in the FWC will have six typical modes such as plunging, twisting, pitching, rolling, and two swing modes. The six GVT rigid-body modes in this exercise are quite similar to figures in the previous work [6]. Figure 6 show the four lowest structural modes: first symmetric, first antisymmetric bending, and two torsional modes. (Counterparts for the CAC are given in Figs. 7 and 8.) The associated eigenmodes are described in Tables 5 and 6.

In the CAC, some of the GVT rigid-body modes match those of the FWC, and the four lowest elastic modes appear in both configurations. However, the fuselage, tip mass, and additional bungee cord attached at the tip end of fuselage can lead to an unusual GVT rigid-body mode that can be described as "pitching about the tail." The fuselage inertia and tail mass also contribute to differences in the structural modes, and they will tend to lower the wing torsional mode in the same phase between the right and left tips. Because of the relatively short fuselage length, however, no structural modes of the fuselage appear among the lowest structural modes.

VII. Conclusions

With the development of bungee and multiple-beam formulations, an analysis for simulation of the GVT environment was conducted for both a FWC and a CAC. The GVT analysis provides preliminary information about the existence and makeup of modes dominated by rigid-body motion and their proximity to low-frequency structural modes for given configurations. This will enable one to determine which modes should be targeted in GVT and what condition might be best to widely separate the frequencies of GVT rigid-body modes from those of low-frequency structural modes.

The results obtained showed that the deformed shape of highly flexible wings significantly affects the modal characteristics, especially for some low-frequency structural modes. Thus, for accurate results the deformed shape needs to be considered in the aeroelastic analyses of highly flexible aircraft. This is facilitated by use of a fully nonlinear structural model; a single modal description cannot describe accurately large deflections for highly flexible aircraft. In addition, some of the structural modes are observed to be affected by the locations of bungee cords, especially if a bungee cord is attached to a wing at a point where the largest displacement of a mode of interest mode occurs. Its location also should be chosen carefully to extract modal frequencies dominated by structural deformation for the free–free boundary condition. Otherwise, it is inevitable that the GVT rigid-body mode induced by bungee systems will couple significantly with low-frequency structural modes.

Acknowledgments

This work was supported in part by the NASA Dryden Flight Research Center, with Kevin Walsh as the technical monitor. Technical discussions with Dana Taylor of Aerovironment, Inc., are gratefully acknowledged.

References

[1] van Schoor, M. C., and von Flotow, A. H., "Aeroelastic Characteristics of a Highly Flexible Aircraft," *Journal of Aircraft*, Vol. 27, No. 10, Oct. 1990, pp. 901–908.

[2] Kehoe, M. W., "Aircraft Ground Vibration Testing at NASA Ames-Dryden Flight Research Facility," NASA TM-88272, July 1987.

[3] Hodges, D. H., "A Mixed Variational Formulation Based on Exact Intrinsic Equations for Dynamics of Moving Beams," *International Journal of Solids and Structures*, Vol. 26, No. 11, 1990, pp. 1253–1273.

[4] Hodges, D. H., "Geometrically-Exact, Intrinsic Theory for Dynamics of Curved and Twisted Anisotropic Beams," *AIAA Journal*, Vol. 41, No. 6, June 2003, pp. 1131–1137.

[5] Hodges, D. H., *Nonlinear Composite Beam Theory*, AIAA, Reston, VA, 2006, Article 5.IV.

[6] Chang, C.-S., and Hodges, D. H., "Modeling of Ground Vibration Testing for Highly Flexible Aircraft," *Proceedings of the 47th Structures, Structural Dynamics, and Materials Conference*, AIAA, Reston, VA, May 2006.

[7] Kovacs, I., and Voros, G., "On the Mathematical Description of the Tensile Stress-Strain Curves of Polycrystalline Face Centered Cubic Metals," *International Journal of Plasticity*, Vol. 12, No. 1, 1996, pp. 35–43.

[8] Tsukrov, I., Eroshkin, O., Paul, W., and Celikkol, B., "Numerical Modeling of Nonlinear Elastic Components of Mooring Systems," *IEEE Journal of Oceanic Engineering*, Vol. 30, No. 1, Jan. 2005, pp. 37–46.

[9] James, A. G., Green, A., and Simpson, G. M., "Strain Energy Functions of Rubber. 1. Characterization of Gum Vulcanizates," *Journal of Applied Polymer Science*, Vol. 19, No. 7, 1975, pp. 2033–2058.

[10] Ogden, R. W., "Large Deformation Isotropic Elasticity—On the Correlation of Theory and Experiment for Incompressible Rubberlike Solids," *Proceedings of the Royal Society of London A*, Vol. 326, No. 1567, Feb. 1972, pp. 565–584.

[11] Arruda, E. M., and Boyce, M. C., "A Three-Dimensional Constitutive Model for the Large Stretch Behavior of Rubber Elastic Materials,"

Journal of the Mechanics and Physics of Solids, Vol. 41, No. 2, Feb. 1993, pp. 389–412.

[12] Anand, L., "On H. Hencky's Approximate Strain-Energy Function for Moderate Deformations," *Journal of Applied Mechanics*, Vol. 46, March 1979, pp. 78–82.

[13] Degener, M., Hodges, D. H., and Petersen, D., "Analytical and Experimental Study of Beam Torsional Stiffness With Large Axial Elongation," *Journal of Applied Mechanics*, Vol. 55, March 1988, pp. 171–178.

[14] Kienholz, D. A., Crawley, E. F., and Harvey, T. J., "Very Low Frequency Suspension Systems for Dynamic Testing," *Proceedings of the 30th Structures, Structural Dynamics and Materials Conference*, AIAA, Washington, D.C., 3–5 April 1989, pp. 327–336.

[15] Teter, J. E., Jr., "A Discussion of Zero Spring Rate Mechanisms Used for the Active Isolation Mount Experiment," NASA TM 209723, Langley Research Center, 1999.

[16] Woodard, S. E., and Housner, J. M., "Nonlinear Behavior of a Passive Zero-Spring-Rate Suspension System," *Journal of Guidance, Control, and Dynamics*, Vol. 14, No. 1, 1991, pp. 84–89.

[17] Mays, T. W., Plaut, R. H., and Liapis, S. I., "Three-Dimensional Analysis of Submerged, Moored, Horizontal, Rigid Cylinders Used as Breakwaters," *Ocean Engineering*, Vol. 26, No. 12, 1999, pp. 1311–1333.

[18] Shiang, W.-J., Cannon, D., and Gorman, J., "Dynamic Analysis of the Cable Array Robotic Crane," *Proceedings of the 1999 IEEE International Conference on Robotics and Automation*, IEEE, Piscataway, NJ, 1999, pp. 2495–2500.